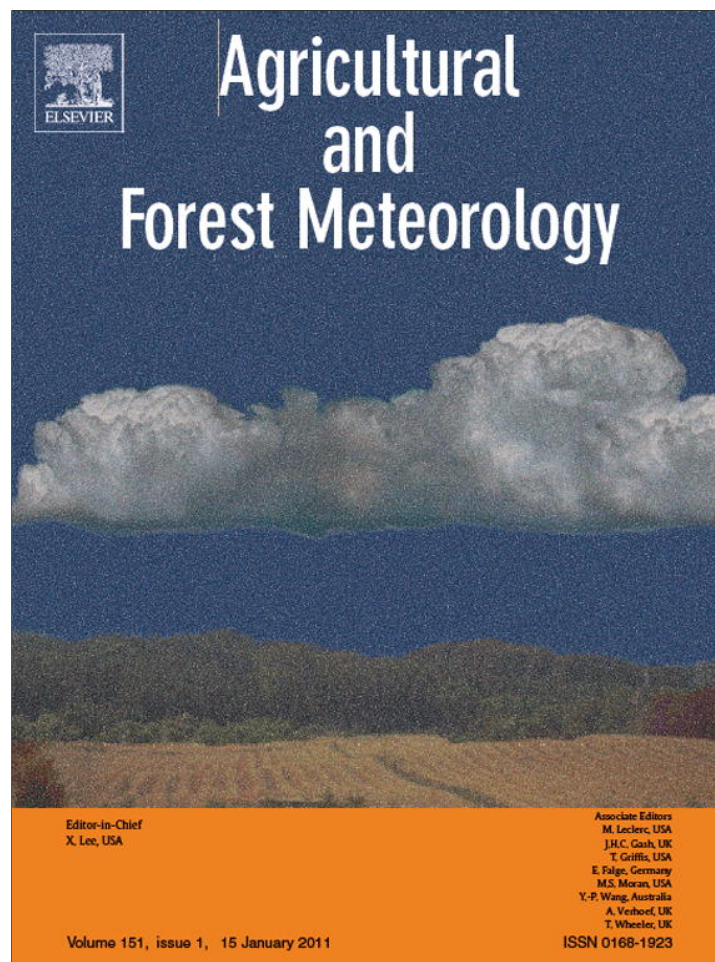


Provided for non-commercial research and education use.
Not for reproduction, distribution or commercial use.



(This is a sample cover image for this issue. The actual cover is not yet available at this time.)

This article appeared in a journal published by Elsevier. The attached copy is furnished to the author for internal non-commercial research and education use, including for instruction at the authors institution and sharing with colleagues.

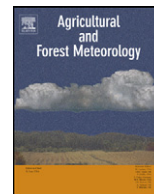
Other uses, including reproduction and distribution, or selling or licensing copies, or posting to personal, institutional or third party websites are prohibited.

In most cases authors are permitted to post their version of the article (e.g. in Word or Tex form) to their personal website or institutional repository. Authors requiring further information regarding Elsevier's archiving and manuscript policies are encouraged to visit:

<http://www.elsevier.com/copyright>

Contents lists available at [SciVerse ScienceDirect](http://www.elsevier.com/locate/agrformet)

Agricultural and Forest Meteorology

journal homepage: www.elsevier.com/locate/agrformet

An alternative method using digital cameras for continuous monitoring of crop status

Toshihiro Sakamoto^{a,b,*,1}, Anatoly A. Gitelson^b, Anthony L. Nguy-Robertson^b, Timothy J. Arkebauer^c, Brian D. Wardlow^b, Andrew E. Suyker^b, Shashi B. Verma^b, Michio Shibayama^a

^a Ecosystem Informatics Division, National Institute for Agro-Environmental Sciences, Tsukuba, Ibaraki, Japan

^b School of Natural Resources, University of Nebraska-Lincoln, Lincoln, NE, USA

^c Department of Agronomy and Horticulture, University of Nebraska-Lincoln, Lincoln, NE, USA

ARTICLE INFO

Article history:

Received 6 July 2011

Received in revised form 17 October 2011

Accepted 21 October 2011

Keywords:

Exposure value

Nighttime flash images

Crop phenology

MODIS

Radiometer

Vegetation index

ABSTRACT

Crop physiological and phenological status is an important factor that characterizes crop yield as well as carbon exchange between the atmosphere and the terrestrial biosphere in agroecosystems. It is difficult to establish high frequency observations of crop status in multiple locations using conventional approaches such as agronomical sampling and also remote sensing techniques that use spectral radiometers because of the labor intensive work required for field surveys and the high cost of radiometers designed for scientific use. This study explored the potential utility of an inexpensive camera observation system called crop phenology recording system (CPRS) as an alternative approach for the observation of seasonal change in crop growth. The CPRS consisting of two compact digital cameras was used to capture visible and near infrared (NIR) images of maize in 2009 and soybean in 2010 for every hour both day and night continuously. In addition, a four channel sensor SKYE measured crop reflectance and Moderate Resolution Imaging Spectroradiometer (MODIS) satellite images were acquired over crop fields. The six different camera- radiometer- and MODIS-derived vegetation indices (VIs) were calculated and compared with the ground-measured crop biophysical parameters. In addition to VIs that use digital numbers, we proposed to use daytime exposure value-adjusted VIs. The camera-derived VIs were compared with the VIs calculated from spectral reflectance observations taken by SKYE and MODIS. It was found that new camera-derived VIs using daytime exposure values are closely related to VIs calculated using SKYE and MODIS reflectance and good proxies of crop biophysical parameters. Camera-derived green chlorophyll index, simple ratio and NDVI were found to be able to estimate the total leaf area index (LAI) of maize and soybean with high accuracy and were better than the widely used 2g-r-b. However, camera-derived 2g-r-b showed the best accuracy in estimating daily fAPAR in vegetative and reproductive stages of both crops. Visible atmospherically resistant vegetation index showed the highest accuracy in the estimation of the green LAI of maize. A unique VI, calculated from nighttime flash NIR images called the nighttime relative brightness index of NIR, showed a strong relationship with total aboveground biomass for both crops. The study concludes that the CPRS is a practical and cost-effective approach for monitoring temporal changes in crop growth, and it also provides an alternative source of ground truth data to validate time-series VIs derived from MODIS and other satellite systems.

© 2011 Elsevier B.V. All rights reserved.

1. Introduction

In recent years, there have been many attempts to use remote sensing techniques to quantitatively assess seasonal changes in vegetation growth in order to estimate phenological and physiological status of vegetation, predict yield, and understand the

temporal features of carbon exchange between the atmosphere and the terrestrial biosphere. There is increasing momentum toward the expansion of the phenology network in Japan, Phenological Eye Network (Nishida, 2007) and the United States, National Phenology Network (NPN) (Betancourt et al., 2005). There are several tower flux observation sites, where both downwelling and upwelling light is measured using automatically rotating custom-ordered spectral radiometers coupled with color digital cameras (Motohka et al., 2010; Nagai et al., 2010; Nishida, 2007). However, unlike the weather monitoring network, it is difficult to accumulate fixed point spectral reflectance observations of crop growth in multiple locations because of the high cost of spectral radiometers designed

* Corresponding author at: 3-1-3 Kannondai, Tsukuba, Postal code: 305-8604, Ibaraki, Japan. Tel.: +81 29 838 8228.

E-mail address: sakamt@affrc.go.jp (T. Sakamoto).

¹ JSPS Postdoctoral Fellow for Research Abroad.

for scientific use. Alternatively, seasonal changes in vegetation is investigated using low to moderate resolution satellite sensors in various ecosystems, including natural vegetation (e.g., forests) and crops. Commonly used satellite sensors include National Oceanic and Atmospheric Administration (NOAA)/Advanced Very High Resolution Radiometer (AVHRR) (Reed et al., 1994; Schwartz et al., 2002; White et al., 1997), SPOT/VEGETATION (Brown and de Beurs, 2008; Delbart et al., 2005; Xiao et al., 2004), and Terra/Moderate Resolution Imaging Spectroradiometer (MODIS) (Islam and Bala, 2008; Sakamoto et al., 2005, 2010b, 2011; Wardlow et al., 2006; Zhang et al., 2003). For satellite sensor-based high frequency observations, the observed time-series vegetation index (VI) profile will include various noise components caused by cloud coverage and/or mixed pixel effects because of low to moderate spatial resolution of the sensor (250 m to 1 km per pixel). Moreover, the lack of ground-level observations of vegetation biophysical parameters makes it difficult to interpret the temporal and spatial features of satellite-derived VIs in reference to seasonal changes in the biophysical parameters of vegetation. Because of this situation, many alternative low-cost methods are proposed for continuous monitoring vegetation phenology (Gamon, 2010). One of the less costly methods used photodiodes, Ryu et al. (2010) developed two-band spectral sensor using light emitting diodes (LEDs) to monitor vegetation reflectance. Garrity et al. (2010) developed a four-band filtered photodiode-based sensor system (Quadpd) for continuous measurement of the normalized difference vegetation index (NDVI) and the photochemical reflectance index (PRI) over vegetated canopies. The use of digital cameras is also becoming popular, especially in CO₂ tower flux monitoring sites for interpreting the seasonal variability of the gross primary production (Ahrends et al., 2009; Nishida, 2007; Richardson et al., 2007; Rundel et al., 2006). Most digital cameras are designed to operate in a simple manner so that scenes can be easily saved in the form of photographs. Because digital cameras precisely record the appearance of photographic subjects in a non-destructive manner, they can also be considered to be remote sensing devices that objectively evaluate the visual characteristics of a subject. High-performance compact digital cameras are currently available for less than 200 US dollars. The most recent camera models have various features, including high-resolution imaging elements, high ISO sensitivity, low power consumption, underwater photography functions, large storage capacity of a Secure Digital High-Capacity Card, and an optical adjustment mechanism. These features enable anyone to take good pictures, even if they have no specialized knowledge or skills related to photography. The camera parameters, including aperture and shutter speed, are automatically optimized to control the incoming incident light intensity on the charge-coupled device imaging element in response to the various illumination conditions. Although the camera-based optical method is no match for the photodiodes-based optical method in terms of cost, it has the advantage that a single digital color image itself enables visual assessment of vegetation appearance, such as vegetation fraction, leaf color and plant type.

In agriculture, there has been a great deal of research on the practical utilization of digital camera images for crop management, for example, plant species identification (Meyer et al., 1999), weed detection (Perez et al., 2000), crop growth diagnosis in terms of vegetative fraction (Lukina et al., 1999; Woebbecke et al., 1995), leaf area index (LAI) (Demarez et al., 2008; Shibayama et al., 2011), leaf color (Adamsen et al., 1999; Shibayama et al., 2009a), and nitrogen content (Matsuda et al., 2003; Shibayama et al., 2009b).

Sakamoto et al. (2010a) devised a low-cost camera observation system called the crop phenology recording system (CPRS) to estimate seasonal changes in the biophysical parameters of rice, barley, and maize using daytime red, green, and blue

(RGB) and nighttime-flash near-infrared (NIR) images. However, it remains unknown if camera-derived VIs are comparable to ground-observed VIs, retrieved from reflectance data (measured upwelling and downwelling radiation), or from frequent observations based on moderate resolution satellite sensors.

The goal of this study is to verify the practical effectiveness of CPRS for estimating crop biophysical parameters such as green and total LAI and dry biomass, and its ability for crop monitoring. We compared camera-derived observations with reflectance data measured by 4-band SKYE radiometer, as well as with MODIS data. This study explores and test performance of new camera-derived VIs using exposure values (EV) of daytime RGB and NIR images, calculated from camera parameters, for estimating the biophysical parameters of maize and soybean.

2. Materials and methods

2.1. Experimental field and crops

The experimental field is located at the University of Nebraska-Lincoln (UNL) Agricultural Research and Development Center near Mead, Nebraska, USA (41°10'46.8"N, 96°26'22.7"W), where CO₂ fluxes have been measured since 2001 as part of the Carbon Sequestration Program (Verma et al., 2005). The total area of this non-irrigated field (called site 3) is approximately 60 ha. The test crops for 2009 and 2010 were maize (cultivar: Pioneer 33T57) and soybeans (cultivar: Pioneer 93M11), respectively.

Maize was planted on April 22–23 [DOY: 112–113] in 2009. The key developmental stages of maize were observed as follows: V1 (beginning vegetative stage) on May 20 [DOY: 140], R1 (silking stage) on July 13 [DOY: 194], R4 (dough stage) on August 10 [DOY: 222], R5 (dent stage) on August 13–28 [DOY: 225–240], and R6 (mature stage) on September 14 [DOY: 257]. The agronomic survey for maize, in which LAI and dry biomass weight of each organ (green leaf, dead leaf, stem, and reproductive organ) was measured, was conducted 14 times from May 21 [DOY: 141] to September 9 [DOY: 252] in 2009. The planting date of soybean was May 19 [DOY: 139] in 2010. The key developmental stages of soybean were observed as follows: V1 (beginning vegetative stage) on July 11 [DOY: 162], R1 (beginning bloom) on July 1 [DOY: 182], R4 (full pod) on August 6 [DOY: 218], R5 (beginning seed) on August 13 [DOY: 225], R6 (full seed) on September 3 [DOY: 246], and R7 (beginning maturity) on October 1 [DOY: 274]. The agronomic survey for soybean was also conducted 10 times from June 15 [DOY: 166] to October 1 [DOY: 274] in 2010, however, we did not use the data obtained on the final day of agronomic survey, October 1 [DOY: 274]. Due to a hailstorm that caused blackouts around the experimental field, the fixed point observations using SKYE were stopped on September 13 [DOY: 256] 2010. Spectral and agronomic data during late-September and early-October period was not critical to this study because the soybean canopy was fully senesced and became leafless during this period prior to harvest, which was well beyond the targeted vegetative and early reproductive growth stages in this study.

Measurements of photosynthetically active radiation (PAR) were obtained using the following procedures: Incoming PAR (PAR_{inc}) was measured with Li-Cor (Lincoln, NE) point quantum sensors pointing to the sky, and placed at 6 m from the ground. PAR reflected by the canopy and soil (PAR_{out}) was measured with Li-Cor point quantum sensors pointing down, and placed at 6 m above the ground. PAR transmitted through the canopy (PAR_{transm}) was measured with Li-Cor line quantum sensors placed at about 2 cm above the ground, looking upward; PAR reflected by the soil (PAR_{soil}) was measured with Li-Cor line quantum sensors placed about 12 cm above the ground, looking downward (details by Hanan et al., 2002;

Viña and Gitelson, 2005). Absorbed PAR (APAR) was calculated as:

$$\text{APAR} = \text{PAR}_{\text{inc}} - \text{PAR}_{\text{out}} - \text{PAR}_{\text{transm}} + \text{PAR}_{\text{soil}}$$

$f\text{APAR}$ was calculated as $\text{APAR}/\text{PAR}_{\text{inc}}$.

Daily fraction of absorbed photosynthetically active radiation ($f\text{APAR}$) was calculated from hourly averages of radiant fluxes.

2.2. Instruments monitoring the experimental field

2.2.1. Crop phenology recording system (CPRS)

Two Nikon COOLPIX P5100 (Nikon Corporation, Tokyo, Japan) digital cameras were utilized in the CPRS (Sakamoto et al., 2010a). One camera was used to capture color images without any hardware modification. In this paper, this camera is called the “RGB-cam.” The other camera was modified to capture NIR images by removing an NIR-cut filter inside the camera body and attaching an NIR band-pass filter on the camera lens. This camera is referred to as the “NIR-cam.” The center wavelength of the NIR band-pass filter was 830 nm. Both cameras were protected by custom-made waterproof cases. The CPRS was connected to a 120 V AC power supply through a handmade uninterruptible power system (UPS) consisting of a lead battery and AC–DC and DC–DC converters. This UPS worked well as a reserve power source when a massive power outage resulted from a hailstorm in Mead on September 13 [DOY: 256] 2010. The CPRS continued to capture RGB and NIR images following the hailstorm damage on the experimental field.

Whereas many phenological studies install the camera for off-nadir sampling to observe a great range of vegetation phenology, the CPRS was installed on top of a custom-made camera station to view in the downward direction (nadir sampling) in accord with standard radiometric remote sensing measurements. Because the CPRS was designed to estimate biophysical variables such as LAI, this study employed the nadir sampling to minimize the impact of view-zenith angle for quantitatively reflecting area of vegetation and uncovered soil surface in the vegetation index. Although the installation height was changed from 3.59 m in 2009 to 3.4 m in 2010, there was not much difference in the footprint area of the camera viewing field at ground level (3.53×2.65 m in 2009 and 3.46×2.59 m in 2010). The RGB and NIR-cams were both set to the “program auto mode”, which adjusts the exposure time (shutter speed) and F-stop (aperture) optimally. Both cameras automatically captured hourly RGB and NIR images in the interval-shooting mode. A built-in flash device was used to capture nighttime flash NIR images under the camera setting called “auto flash mode.” Other camera settings were as follows: “QXGA (3.1 megapixels; 2048 pixels \times 1536 pixels)” for recording image size, “FINE (image compression rate: 25%)” for image quality, “cloud” for auto-white balance, and “auto” for ISO sensitivity. The observation periods of the CPRS were from May 9 [DOY: 129] to November 17 [DOY: 321] in 2009 and from April 22 [DOY: 145] to October 17 [DOY: 290] in 2010. The time-series daytime RGB images of maize and soybean are shown in Fig. 1.

2.2.2. Four-band SKYE radiometers

Two four-band light sensors (SKR 1850, ©Skye Instruments Ltd, Llandrindod Wells, UK) were used in this study. The spectral bands were as following: 536.5–561.5 nm (green), 664.5–675.5 nm (red), 704.5–715.5 nm (red edge), and 862–874 nm (NIR). The SKYE sensors were installed at a fixed height of 6 m above the ground to measure the spectral irradiance of downward incident light (with cosine collector attached) and the upward radiance reflected by the canopy every 30 min from 500 to 1900 h. Since the SKYE sensors have a 25° field of view, the footprint size was approximately 3 m in diameter at ground level. The observation periods using the

SKYE sensor were from May 11 [DOY: 131] to October 7 [DOY: 280] in 2009 and from April 22 [DOY: 112] to September 12 [DOY: 255] in 2010. Reflectance was calculated as a ratio of upwelling radiance to downwelling irradiance.

2.3. MODIS data

This study used an eight-day timeseries of 250 m and 500 m MODIS surface reflectance data (MOD09Q1 and MOD09A1, Collection 5, tile: h10v04) acquired by MODIS on board Terra in the 2009 and 2010 growing seasons. The MODIS eight-day composite product was corrected for atmospheric effects, providing the best surface spectral-reflectance data for each eight-day period using the constrained view-angle maximum value composite method (Huete et al., 2002). The MOD09Q1 includes only the 250 m red (Band 1, 620–670 nm) and near-infrared (Band 2, 841–876 nm) reflectance data. The 500 m green reflectance data (Band 4, 545–565 nm) from the MOD09A1 were resampled from 500 to 250 m resolution using the nearest-neighbor method. The dates used in the temporal profile of eight-day values were actual collection dates recorded in the MOD09A1. The selected MODIS-pixel location (single pixel) was the near central of the experimental field and was the same as that used in a previous study, which proposed a new crop phenology detection method for maize and soybean with time-series MODIS data (Sakamoto et al., 2010b).

3. VIs based on CPRS digital camera images

The nonlinear relationship between the digital number (DN) of image pixels and the intensity of incident light, the so-called gamma characteristic of imaging elements, was calibrated by a formula using the expression of degree 6 derived from a laboratory experiment (Matsuda et al., 2003; Sakamoto et al., 2010a). Then, the camera-derived VIs were calculated from the calibrated digital numbers (cDN) of RGB and NIR images through the following procedures. Firstly, all pixels of an hourly image were averaged to obtain hourly-averaged cDN for the red, green, and blue layers of the RGB image. According to the laboratory experiment calibrating the gamma characteristic of the imaging element of the camera, relationship between cDN and relative light intensity was linear when cDN was lower than 100 (Sakamoto et al., 2010a). Then, it was empirically found that the second-layer cDN of the nighttime NIR images had better sensitivity to changes in intensity of NIR light. Therefore, the cDN of second-layer NIR image was assigned as cDN_{NIR} . Daily median cDN was calculated from daytime (10:00–14:00 h) and nighttime (22:00–02:00 h) periods. The exposure value (EV), which is determined from the F-stop (aperture), exposure time (shutter speed) and ISO sensitivity, is one of the important parameters related to varying illumination intensity. However, the daytime EV has seldom been used in previous studies for crop growth observation based on digital camera images. The procedures for calculating EV and exposure value-adjusted cDN (ev-cDN) are as follows:

$$\text{EV} = 2 * \log_2(F) - \log_2(T) - \log_2\left(\frac{\text{ISO}}{64}\right) \quad (1)$$

$$\text{ev-cDN} = \text{cDN} * 2^{\text{EV}} \quad (2)$$

where cDN is the daily median value for the daytime or nighttime period and F, T, and ISO are the aperture (F-stop), exposure time (shutter speed), and ISO sensitivity, respectively, which are recorded in the header region of EXIF-formatted JPEG files in RGB and NIR images. The ISO value of the daytime image always remained at the lowest level of 64. The values of F and T of the nighttime image always remained at 2.7 and 1/60 s, respectively. The











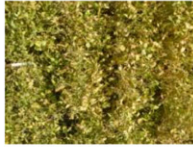
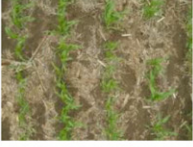






















Date (DOY)	Maize [2009]	Soybean [2010]	Date (DOY)	Maize [2009]	Soybean [2010]
5/20 (140)			8/28 (240)		
5/30 (150)			9/07 (250)		
6/09 (160)			9/17 (260)		
6/19 (170)			9/27 (270)		
6/29 (180)			10/07 (280)		
7/09 (190)			10/17 (290)		
7/19 (200)			10/27 (300)		
7/29 (210)			11/06 (310)		
8/08 (220)			11/16 (320)		
8/18 (230)					

Fig. 1. Time-series digital color images acquired for maize in 2009 and for soybean field in 2010.

dynamic range of ISO was from 64 to 800 at nighttime under flash illumination. For soybean monitoring, the nighttime ISO remained at the highest level of 800 for the entire growing season because the camera-to-object distance was too far to make the built-in flash

device sufficiently illuminate the top of the soybean canopy without the highest level of ISO sensitivity.

Previous studies Sakamoto et al. (2010a, 2011a,b) suggested an advantage of a new concept incorporating the EV into the

camera-derived VI for assessing the three-dimensional character of crop community such as nighttime active remote sensing. The nighttime $ev-cDN_{NIR}$ was called the nighttime relative brightness index of NIR ($NRBI_{NIR}$).

3.1. Camera-derived VIs investigated in the previous study

Sakamoto et al. (2011a) found that the Visible Atmospherically Resistant Index (VARI, Gitelson et al., 2002), two-green-red-blue (2g-r-b, Woebbecke et al., 1995), derived from daytime RGB images, and the Nighttime Relative Brightness Index in NIR ($NRBI_{NIR}$, Sakamoto et al., 2010a), derived from nighttime flash NIR images, had close relationships with the biophysical parameters of maize for the whole growing season. The best camera-derived VIs that showed the highest coefficients of determination between the biophysical parameters were as follows: VARI vs. green LAI (GLAI) and green leaf biomass (GLB), 2g-r-b vs. total LAI (TLAI), and $NRBI_{NIR}$ vs. total dry weight of stems and leaves (SB+TLB). It was also confirmed that VARI had a strong relationship with LAI estimates of paddy rice until the heading stage (Sakamoto et al., 2011b). The $NRBI_{NIR}$ was found to be a good proxy for above-ground dry biomass of paddy rice and the plant height of paddy rice and barley (Sakamoto et al., 2010a).

VARI and 2g-r-b were calculated from daytime cDN_{red} , cDN_{green} , and cDN_{blue} (Eqs. (3) and (4)). $NRBI_{NIR}$ (also called the nighttime $ev-cDN$ of NIR) was calculated using cDN_{NIR} and exposure value (EV) derived from nighttime flash NIR images and these camera parameters (F-stop, shutter speed, and ISO sensitivity) (Eqs. (2) and (5)).

The equations for VARI, 2g-r-b, and $NRBI_{NIR}$ are

$$VARI \text{ (Camera)} = \frac{cDN_{green} - cDN_{red}}{cDN_{green} + cDN_{red}} \quad (3)$$

$$2g-r-b \text{ (Camera)} = 2 \times cDN_{green} - cDN_{red} - cDN_{blue} \quad (4)$$

$$NRBI_{NIR} = ev-cDN_{NIR} \text{ (night)} = cDN_{NIR} \text{ (night)} * 2^{(2 * \log_2(F_{NIR}) - \log_2(T_{NIR}) - \log_2(ISO_{NIR}/64))} \quad (5)$$

where cDN_{green} , cDN_{red} , and cDN_{blue} are derived from the green, red, and blue layers of daytime RGB images, respectively, and cDN_{NIR} (night) is derived from the second layer of nighttime NIR images. F_{NIR} , T_{NIR} , and ISO_{NIR} are derived from the header region of nighttime NIR images captured under flash light.

There are variations of VARI in terms of the selected wavelength and optional usage of the blue band. This study used a VARI without using blue band (see Eq. (1) in Gitelson et al., 2002). In the literature, a vegetation index based on the same equation as Eq. (3) has often used under different names or abbreviations such as “VI = DIF/SUM” (Tucker, 1979), “NDI” (Perez et al., 2000), “GRVI” (Falkowski et al., 2005; Motohka et al., 2010) and “NDVI_{gr}” (Sakamoto et al., 2010a).

3.2. New camera-derived VIs based on daytime exposure value-adjusted cDN

The NDVI based on the NIR and red reflectance (NDVI, Rouse, 1974) is commonly used for assessment of the quality or quantity of vegetation in both close-range and satellite remote sensing. The simple ratio of NIR divided by red reflectance (hereinafter called SR, Jordan, 1969) has also been widely used for vegetation monitoring. The chlorophyll indicator (green chlorophyll index, CI_{green}), which is calculated using green and NIR reflectance, originates from a 3-band model as a special case for sensing total canopy chlorophyll (Gitelson et al., 2005).

As for observations with variable incident radiation based on digital cameras, it is too difficult to calibrate a camera in terms of reflectance. Another approach that uses an additional optical

instrument monitoring skylight illumination loses the advantages of manageability and the low-cost camera observation system. In addition, the spectral sensitivity characteristic of the imaging element used in the digital camera is not disclosed by manufacturers. In this study, we calculated the camera-based NDVI, CI_{green} , and SR directly from daytime $ev-cDN$ of RGB- and NIR-cams. Thus, the newly proposed equations for camera-derived VIs are as follows:

$$ev-NDVI \text{ (Camera)} = \frac{ev-cDN_{NIR} - ev-cDN_{red}}{ev-cDN_{NIR} + ev-cDN_{red}} \quad (6)$$

$$ev-SR \text{ (Camera)} = \frac{ev-cDN_{NIR}}{ev-cDN_{red}} \quad (7)$$

$$ev-CI_{green} \text{ (Camera)} = \frac{ev-cDN_{NIR}}{ev-cDN_{green}} \quad (8)$$

where $ev-cDN_{green}$, $ev-cDN_{red}$, and $ev-cDN_{NIR}$ were calculated from cDN_{green} , cDN_{red} , and cDN_{NIR} coupled with daytime EV_{RGB} and EV_{NIR} using equations ((1) and (2)). Median values calculated from daytime images observed from around 10:00 to 14:00 h were used for the daily profile of each VIs.

3.3. VIs based on spectral reflectance of SKYE and MODIS

We compared the camera-derived VIs, VARI, NDVI, SR, and CI_{green} with VIs calculated with spectral reflectance measured by SKYE and MODIS. The equations of the SKYE- or MODIS-derived VIs are as follows:

$$VARI \text{ (SKYE or MODIS)} = \frac{\rho_{green} - \rho_{red}}{\rho_{green} + \rho_{red}} \quad (9)$$

$$NDVI \text{ (SKYE or MODIS)} = \frac{\rho_{NIR} - \rho_{red}}{\rho_{NIR} + \rho_{red}} \quad (10)$$

$$SR \text{ (SKYE or MODIS)} = \frac{\rho_{NIR}}{\rho_{red}} \quad (11)$$

$$CI_{green} \text{ (SKYE or MODIS)} = \frac{\rho_{NIR}}{\rho_{green}} - 1 \quad (12)$$

where ρ_{green} , ρ_{red} , and ρ_{NIR} are spectral reflectance in bands of SKYE or MODIS.

The MODIS eight-day composite product had only one observation of surface spectral reflectance within a defined eight day period. Therefore, MODIS-derived VIs were linearly interpolated from eight-day intervals to daily intervals between temporally adjacent compositing periods in reference to the observation date (day of year, DOY) recorded in MOD09A for comparing with daily data of camera and SKYE-derived VIs.

4. Results and discussion

4.1. Temporal behavior of spectral reflectance observed by SKYE and MODIS

The seasonal patterns of green, red, and NIR reflectance observed by SKYE (Fig. 2A and B) were in good agreement with those observed by MODIS (Fig. 2C and D) for both maize and soybean. Whereas the green and red reflectance decreased in response to vegetation growth, the NIR reflectance increased in the same periods (DOY 140–190 in 2009 for maize, DOY 150–210 in 2010 for soybeans). Although the seasonal variation of green and red reflectance are similar for the SKYE and MODIS observations for both crop species (maize: 2–15%; soybeans: 2–20%), the maximum NIR reflectance of SKYE (approximately 37% for maize, 51% for soybeans) was 7–13% lower than that of MODIS (approximately 50% for maize, 58% for soybeans). There are many potential factors making it difficult to compare absolute values of measured SKYE and MODIS reflectance, which may include differences in footprint size, view

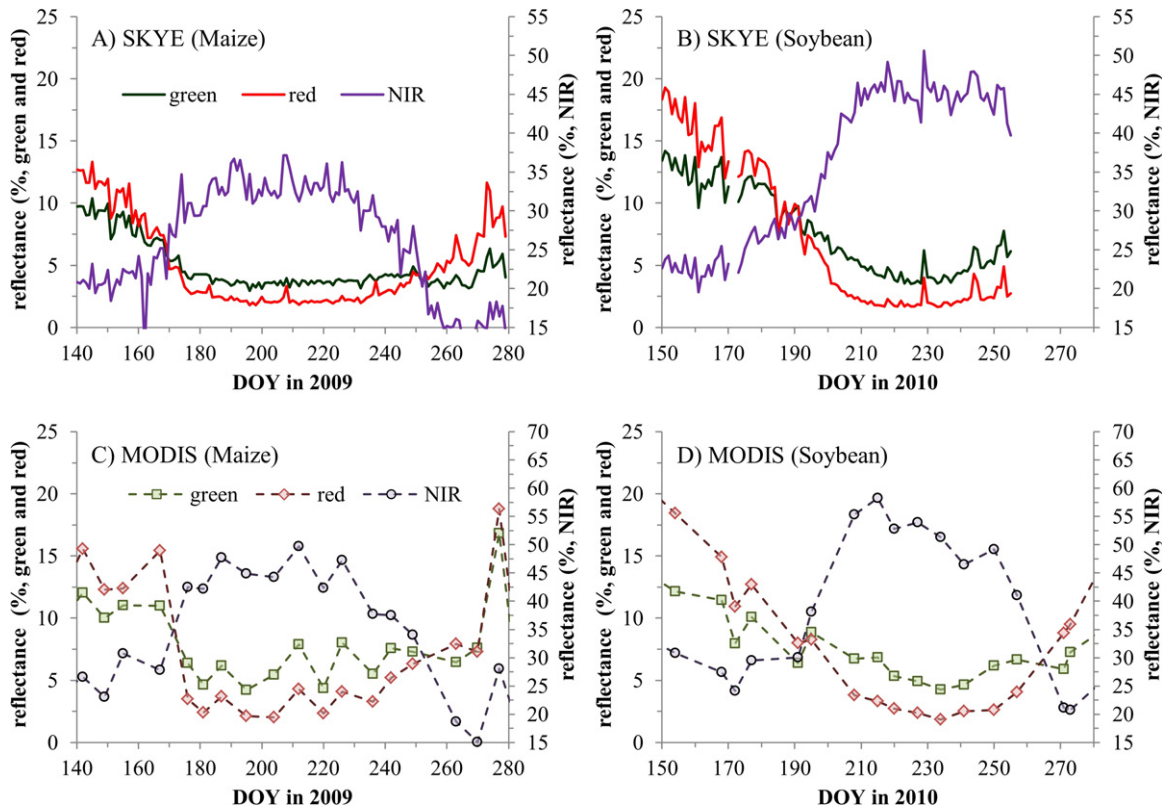


Fig. 2. Temporal profiles of spectral reflectance of maize and soybean field, observed by SKYE sensor (A, B) and MODIS (C, D).

angle, observation frequency, and atmospheric influences between the sensors. It is worth to mention that the difference in the bandwidths of SKYE (25 nm for green, 11 nm for red and 12 nm for NIR) and MODIS (20 nm for green, 50 nm for red, 35 nm for NIR) also affects reflectance values.

4.2. Temporal behavior of the camera values (cDN and ev-cDN)

The time-series profiles of daily median cDN in green, red, blue, and NIR bands are shown in Fig. 3A and B. As found in Sakamoto et al. (2010a), when monitoring paddy rice and barley growth, the seasonal variation of cDN was less than 15 for each band for maize and soybean growth and much smaller than that of spectral reflectance measured by SKYE and MODIS (Fig. 2) with much higher short-term noise components of cDN (Fig. 2A). Temporal behavior of cDN_{green} differs substantially from that of green reflectance of SKYE and MODIS. cDN_{green} increases from the beginning of the growing season while green reflectance showed a decrease that is a fundamental spectral feature of green vegetation. This implies that the seasonal trends of cDN_{green} have no meaning in terms of reflectance properties of crops. While cDN_{red} decreases in the beginning of the season, it increases around DOY 180, in a time period when maize greenness is still increasing. Thus, cDN_{red} also cannot be interpreted in terms of reflectance properties of maize growth.

The temporal profiles of daytime ev-cDN were completely different from those of cDN. Although the daytime $ev-cDN_{green, red, and NIR}$ were more volatile than $cDN_{green, red, and NIR}$ on a daily basis (Fig. 3A–D), the seasonal pattern of each ev-cDN band was similar to that of the spectral reflectance of SKYE and MODIS. Considering that the exposure value (EV) is automatically adjusted with F-stop and shutter speed in accordance with the ever-changing luminous surroundings to regulate the incoming incident light intensity, the daytime ev-cDN can be used as a proxy of upwelling radiance adjusted to incident irradiance. Thus, that

the long-term variability of the ev-cDN time series, which excludes the short-term variation caused by daily weather changes, has a close relationship with the ground-based spectral reflectance observations of SKYE.

The $NRBI_{NIR}$ (nighttime $ev-cDN_{NIR}$) shows characteristic seasonal profiles with fewer short-term fluctuating components for entire crop growing seasons (Fig. 3E and F). This was different from those of the daytime cDN_{NIR} and daytime $ev-cDN_{NIR}$.

4.3. Scatter plots and temporal comparison of camera-derived VIs with SKYE- and MODIS-derived VIs

Table 1 lists determination coefficients, R^2 , for the linear relationships among the VIs calculated with data taken by camera, SKYE, and MODIS. The result reveals that camera-derived ev-VARI, ev-NDVI, ev-SR, and $ev-CI_{green}$ correlated very closely with corresponding SKYE- and MODIS-derived VIs. Relationships between camera-derived ev-VARI, ev-SR and $ev-CI_{green}$ and corresponding SKYE- and MODIS-derived VIs are linear (Fig. 4A). However, relationships between SKYE- and MODIS-derived NDVI vs. camera-derived ev-NDVI tend to saturate above 0.7. This means that camera-derived ev-NDVI is more sensitive to moderate to high vegetation density. This can be explained by the magnitude of the ratio of NIR to red reflectances. The ratio of the camera (ev-SR) reached 3.5 whereas that of SKYE (SR) reached 28 (Fig. 4E and F). One of the reasons of low NDVI sensitivity to moderate to high vegetation density is that the normalization procedure of NDVI, which is the ratio of the difference to the sum (Eq. (10)), makes the NDVI insensitive to variation in the red and NIR reflectance when NIR reflectance is much greater than red-reflectance (the $NIR/red = SR \gg 1$). This occurs as GLAI exceeds $2 m^2/m^2$ (Gitelson, 2004). In contrast, the camera ev-NIR signal is much lower than NIR reflectance of either SKYE or MODIS. Thus, the $ev-cDN_{NIR}/ev-cDN_{red}$ ratio is near 1 and camera-derived ev-NDVI remains sensitive to change in both of

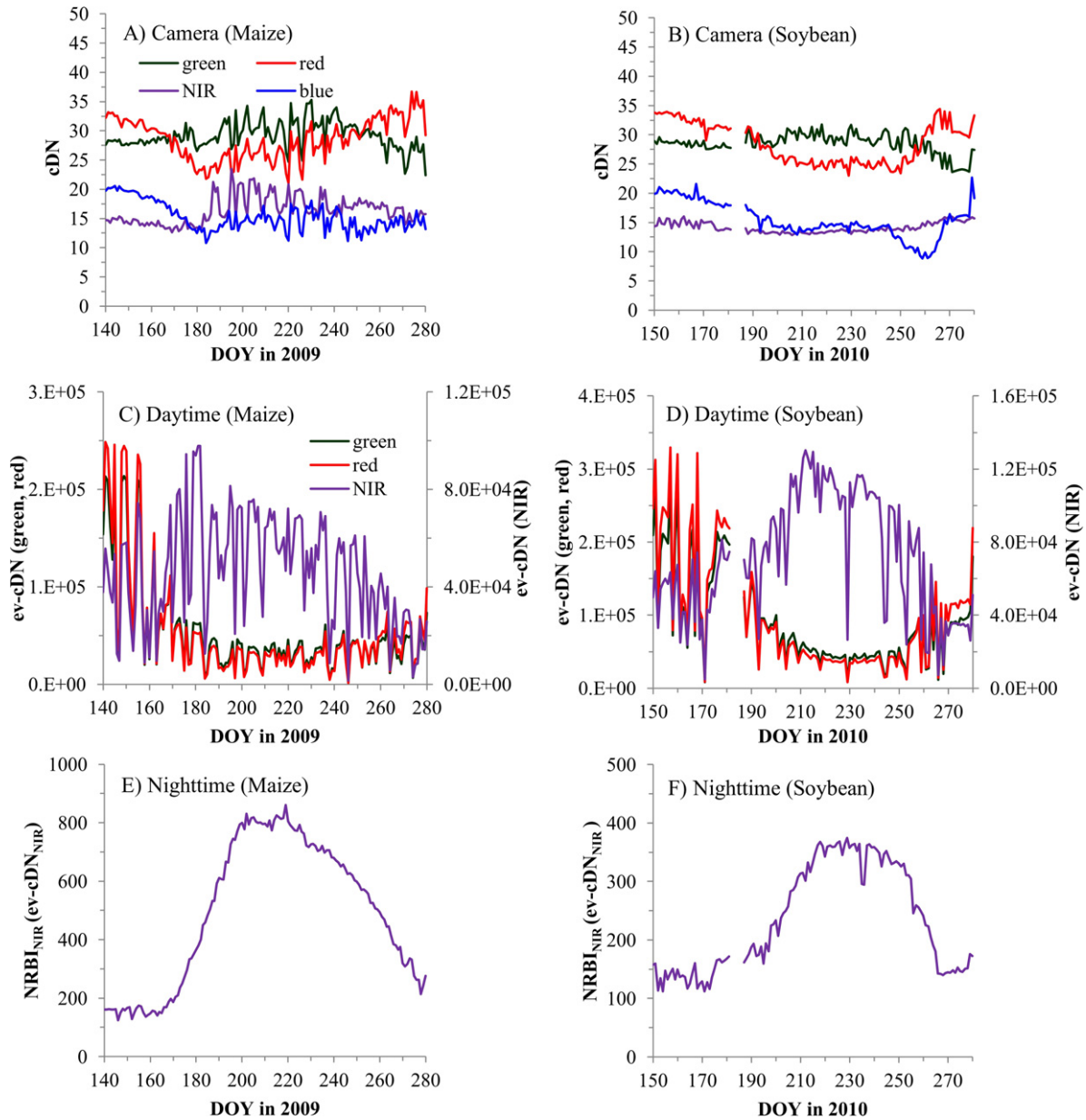


Fig. 3. Temporal profiles of camera-derived values in maize and soybean fields; daytime calibrated digital number (daytime cDN: A, B), daytime exposure value-adjusted cDN (daytime ev-cDN: C, D), and NRBI_{NIR} (also called nighttime ev-cDN_{NIR}: E, F).

Table 1

Determination coefficients, R², of the linear relationships among the VIs derived from the digital camera, SKYE, and MODIS. The comparisons in the same vegetation index between the different sensors are highlighted in bold style.

Explanatory		Observation							
		SKYE				MODIS			
		VARI	NDVI	SR	Cl _{green}	VARI	NDVI	SR	Cl _{green}
Camera	VARI	0.88	0.89	0.71	0.76	0.82	0.91	0.75	0.80
	ev-NDVI	0.80	0.94	0.79	0.89	0.90	0.94	0.80	0.83
	SR	0.81	0.82	0.92	0.93	0.86	0.85	0.89	0.90
	ev-Cl _{green}	0.79	0.82	0.91	0.94	0.85	0.85	0.87	0.88
	2g-r-b	0.78	0.92	0.64	0.74	0.81	0.90	0.67	0.71
	NRBI _{NIR}	0.20	0.39	0.21	0.38	0.43	0.40	0.26	0.24
SKYE	VARI					0.80	0.87	0.78	0.82
	NDVI					0.88	0.94	0.74	0.78
	SR					0.81	0.78	0.87	0.87
	Cl _{green}					0.88	0.85	0.88	0.88

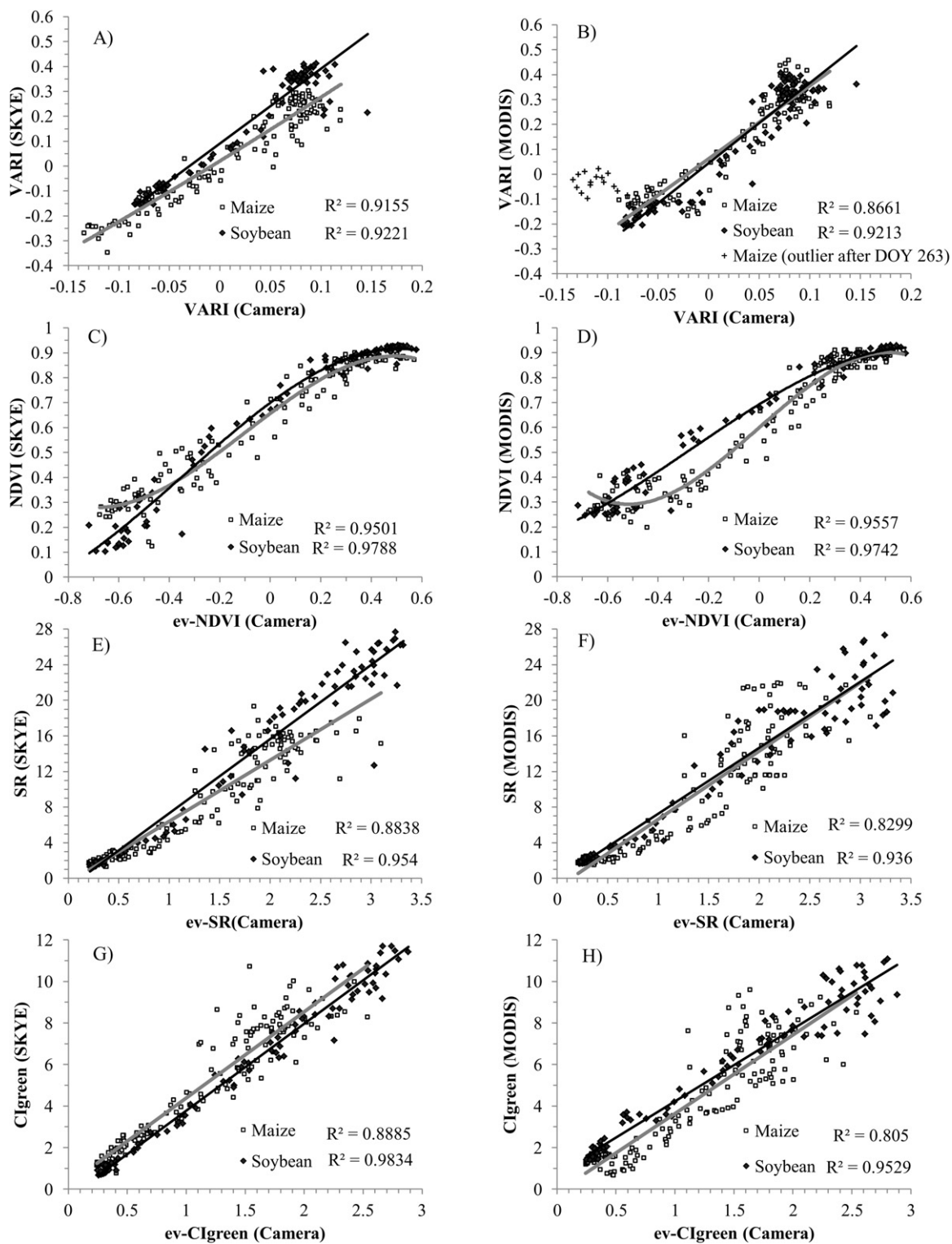


Fig. 4. Comparisons of camera-derived-VIs (VARI, ev-NDVI, ev-SR, and ev- CI_{green}) with the SKYE and MODIS-derived VIs (VARI, NDVI, SR, and CI_{green}) on maize and soybean fields.

the red signal (chlorophyll absorption/crop greenness) and NIR signal (crop density). To achieve the same goal of increasing sensitivity of the NDVI to moderate to high biomass using reflectance data, a weighting coefficient, $a < 1$, was introduced in the Wide Dynamic Range Vegetation Index, WDRVI (Gitelson, 2004). Camera signals $ev-cDN_{red}$ and $ev-cDN_{NIR}$ themselves allow for increase of

efficiency of NDVI without using the weighting coefficient (a) used in WDRVI.

Temporal behaviors of camera, SKYE and MODIS-derived VIs, presented in Figs. 5–8, are almost identical with two exceptions. For maize, camera and MODIS-derived VARI showed pronounced peak at DOY 180–200 (Fig. 5A and C) while SKYE-derived VARI did not.

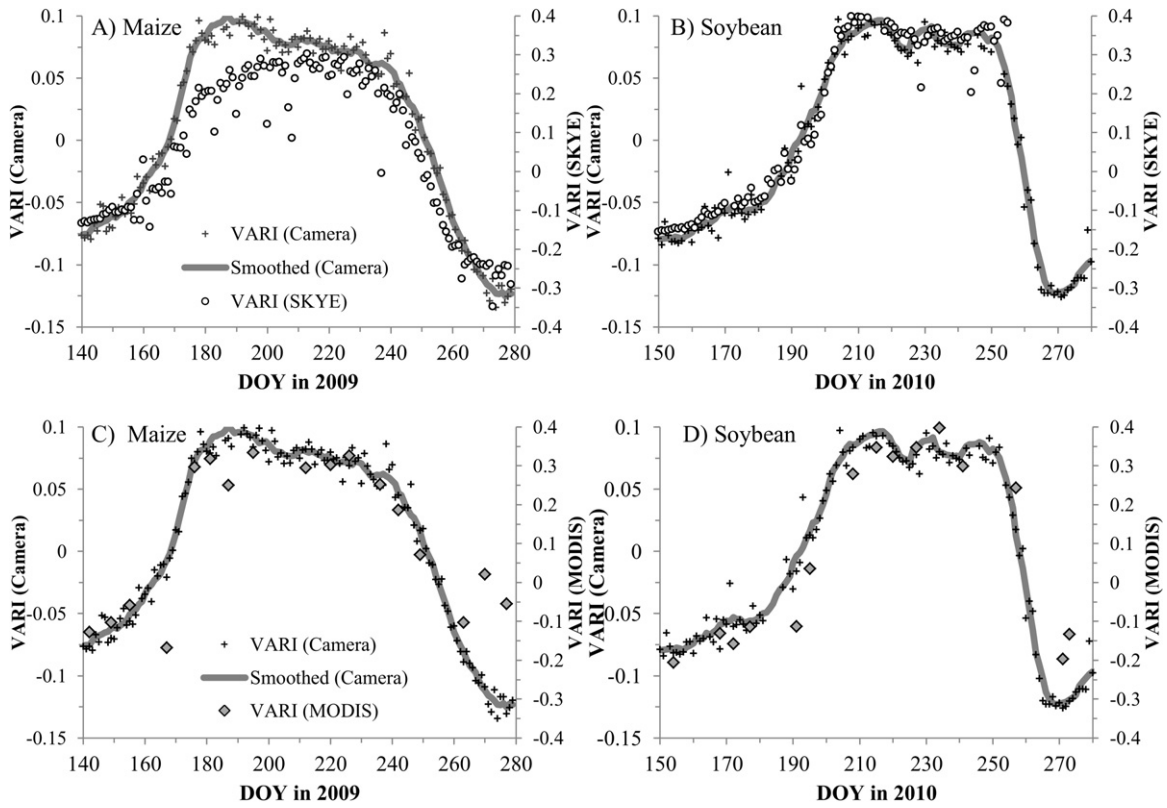


Fig. 5. Temporal comparisons of VARI (Camera) with VARI (SKYE) (A, B) and VARI (MODIS) (C, D).

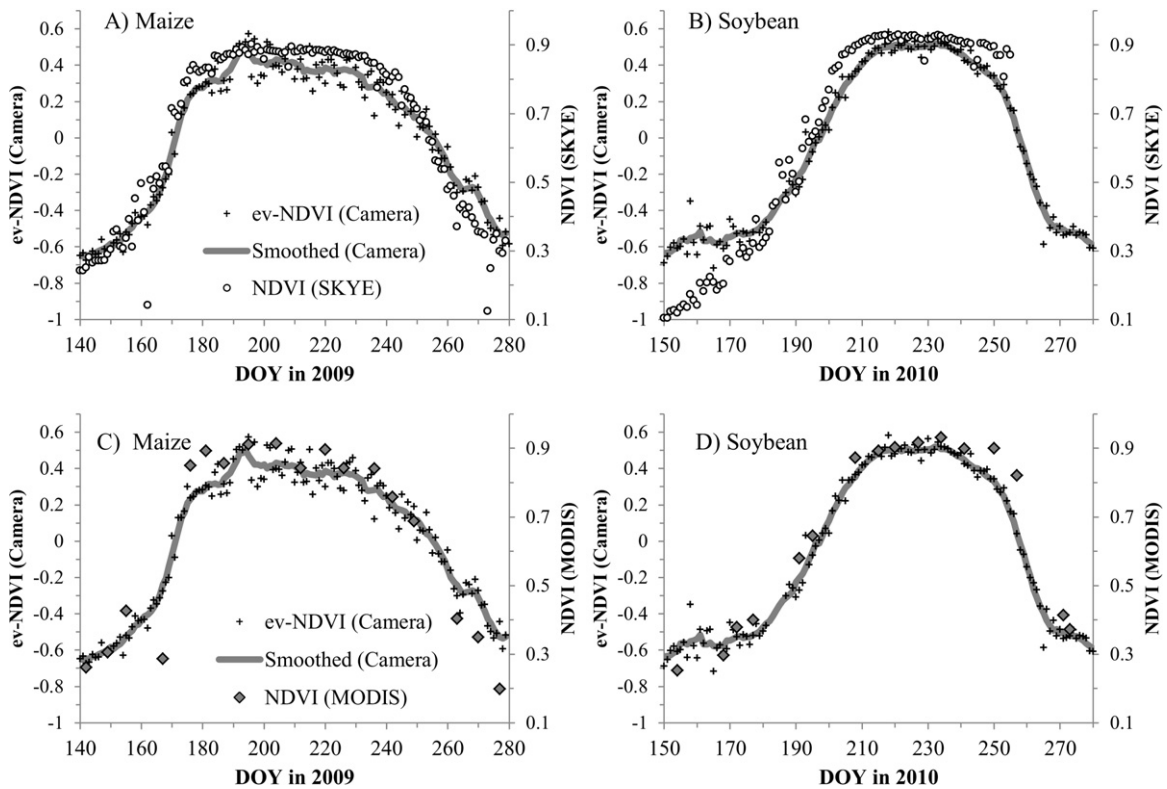


Fig. 6. Temporal comparisons of ev-NDVI (Camera) with NDVI (SKYE) (A, B) and NDVI (MODIS) (C, D).

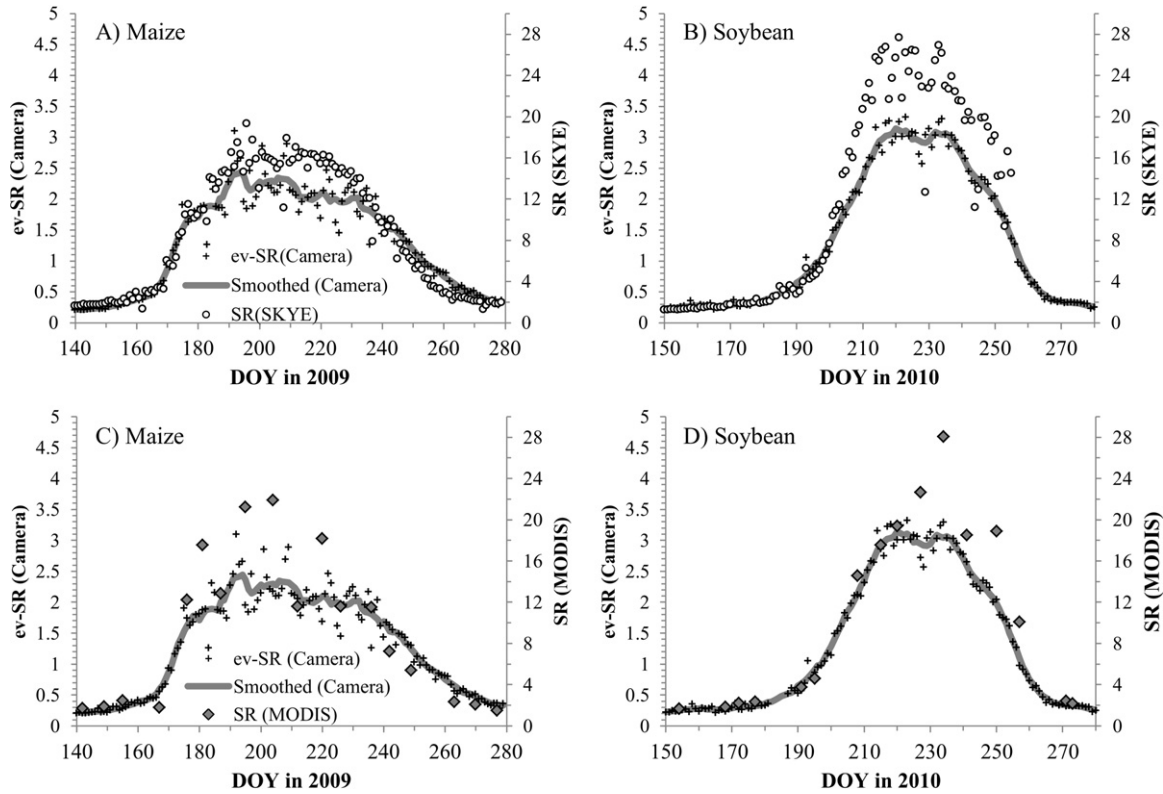


Fig. 7. Temporal comparisons of ev-SR (Camera) with SR (SKYE) (A, B) and SR (MODIS) (C, D).

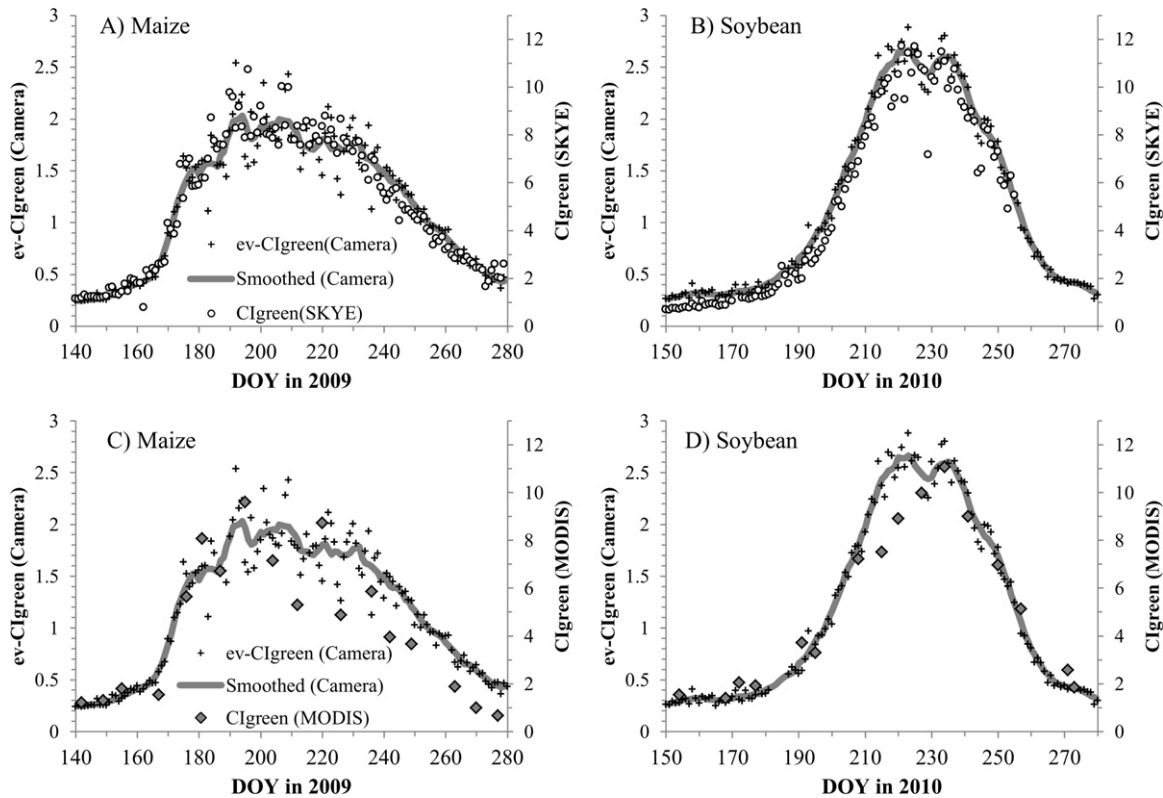


Fig. 8. Temporal comparisons of ev-Clgreen (Camera) with Clgreen (SKYE) (A, B) and Clgreen (MODIS) (C, D).

Table 2

Summary of estimation accuracy (root-mean-square error: RMSE) of camera-, SKYE-, and MODIS-derived VIs used to estimate the seasonal changes in biophysical parameters of maize and soybeans. The best estimation results are highlighted in bold style.

RMSE device	Maize				Soybean				
	VI	GLAI (m ² /m ²)	GLB (kg/ha)	TLAI (m ² /m ²)	SB+TLB (kg/ha)	GLAI (m ² /m ²)	GLB (kg/ha)	TLAI (m ² /m ²)	SB+TLB (kg/ha)
Camera	VARI	0.27	170	0.55	2462	0.40	195	0.40	652
	ev-NDVI	0.51	238	0.23	1754	0.13	85	0.13	349
	ev-SR	0.44	212	0.25	1863	0.12	81	0.11	358
	ev-Cl _{green}	0.53	268	0.20	1717	0.09	79	0.09	353
	2g-r-b	0.69	392	0.30	1934	0.48	234	0.48	772
	NRBI _{NIR}	1.13	624	0.59	457	0.15	24	0.15	109
SKYE	VARI	0.44	202	0.52	2109	0.32	173	0.33	621
	NDVI	0.47	217	0.29	1833	0.24	143	0.24	506
	SR	0.43	182	0.36	1921	0.17	96	0.16	400
	Cl _{green}	0.47	222	0.21	1774	0.07	75	0.07	332
MODIS	VARI	0.51	260	0.46	2051	0.26	106	0.27	265
	NDVI	0.48	227	0.34	1901	0.17	89	0.18	314
	SR	0.28	143	0.55	2354	0.16	67	0.16	145
	Cl _{green}	0.39	208	0.37	2111	0.10	72	0.11	251

According to Vina et al. (2004), VARI is expected to exhibit a conspicuous decrease after maize reached maximal vegetation fraction and GLAI, which corresponds to the appearance of tassels. However, spectral bands of SKYE radiometers used in this study have a very narrow red band (11 nm), while bands of MODIS (50 nm) and a digital camera (larger than 50 nm, Hunt et al., 2010) are much wider. Thus, saturation of reflectance in the red band at maximal maize density explains lower sensitivity of SKYE-derived VARI compared to either camera or MODIS. Another conspicuous difference is between camera and SKYE-derived SR for soybean (Fig. 7B). With reference to seasonality of ev-SR (camera), the SR (SKYE) is higher than ev-SR (camera) in the middle of the crop growing seasons. This is related to the effect mentioned above that the ratio of ev-cDN_{NIR} to ev-cDN_{red} is lower than that of NIR to red reflectance of SKYE, and also to a narrow red band of SKYE than that of the camera. This feature is pronounced in soybean more than in maize (see Fig. 7A and B).

The seasonal patterns of ev-Cl_{green} matched those of Cl_{green} (SKYE) in both maize and soybean (Fig. 8A and B). The scatter plots of ev-Cl_{green} showed strong linear relationships with Cl_{green} from both SKYE and MODIS (Fig. 4G and H). The regression lines of ev-Cl_{green} against Cl_{green} (SKYE) (Fig. 4G) were species independent, unlike those of ev-SR against SR (SKYE) (Fig. 4E). However in a precise sense, there were differences between the seasonal patterns of ev-Cl_{green} and Cl_{green} (MODIS) during the late vegetative stage (DOY 210–230 in 2010) and the senescence stage of maize (DOY 230–280 in 2009). There is a possibility that MODIS-derived Cl_{green} is more likely to be affected by mixed-pixel effects caused by using lower spatial-resolution (500 m) MODIS surface reflectance product for green band than red and NIR bands (250 m). For the same reason mentioned above, the lower NIR/green reflectance ratio of SKYE (up to 13, Fig. 4G and Eq. (12)) makes Cl_{green} (SKYE) much more sensitive to moderate to high vegetation density than SR (SKYE), resulting in the strong linear relationships between ev-Cl_{green} and Cl_{green} (SKYE). Considering that the spectral radiometer-derived Cl_{green} provided an accurate estimation of the total canopy chlorophyll of maize and soybeans (Gitelson et al., 2005), ev-Cl_{green} seems to be a good indicator of seasonal changes in the total canopy chlorophyll content.

4.4. Estimation accuracy of biophysical parameters for maize and soybean

According to Sakamoto et al. (2011a), camera-derived VARI was able to accurately estimate the (GLAI) and (GLB) of maize whereas the 2g-r-b was more accurate in estimating TLAI. In

addition, NRBI_{NIR} (nighttime ev-cDN_{NIR}) showed the highest accuracy in the estimation of the total dry weight of the stalks and leaves of maize. This study assessed the effectiveness of these VIs for soybean as well as for maize. When comparing with the biophysical parameters, VIs derived from camera and SKYE were linearly interpolated to fill missing observations, which were caused by data retrieving and temporary relocation of the camera station due to pesticide spraying and harvesting. Then, a seven-day moving average was applied to smooth the effects of short-term variable noise components, which are assumed to be caused by the ever-changing outdoor illumination conditions and mixed-pixel effects in the temporal profiles of VIs derived from camera, SKYE, and MODIS.

Root mean square error (RMSE) of biophysical parameters estimation of maize and soybean by VIs derived from camera, SKYE, and MODIS are presented in Table 2. In soybean, ev-VARI had poor sensitivity to green LAI > 1.5 (after DOY 202 in 2010) (Fig. 9A). Another finding of this study is that ev-Cl_{green}, ev-SR, and ev-NDVI were much more effective for estimating the TLAI of both crops than the 2g-r-b (Fig. 9B, Table 2). The RMSE of the TLAI estimation by ev-Cl_{green} is comparable to or lower than those of the SKYE and MODIS-retrieved Cl_{green}. The accuracy of green LAI estimation in vegetative and reproductive stages (until DOY 246 R6 stage) in soybean by ev-Cl_{green} was better than that of ev-VARI. This is in contrast to maize where ev-Cl_{green} performed poorly. In senescence, green LAI in soybean decreases drastically and it prevents its accurate estimation. Thus, it is recommended to use camera-derived ev-VARI for estimating the green LAI for the whole growing season of maize and ev-Cl_{green} in vegetative and reproductive stages (until around R6 stage) of soybean.

There is a poor correlation ($R^2 < 0.5$) between NRBI_{NIR} and any other VIs derived from SKYE and MODIS (Table 1). This means that the information content of NRBI_{NIR} (Fig. 3E and F) is different from that of other VIs such as VARI, NDVI, SR, and Cl_{green}. In maize (Sakamoto et al. 2011a), NRBI_{NIR} showed the highest estimation accuracy of the SB+TLB of soybeans (Table 2, Fig. 9C). The fixed point observation for soybean growth showed that the nighttime ISO sensitivity of both RGB- and NIR-cams stayed at its highest level (800) for the entire growing season. This means that the variability of nighttime ISO sensitivity did not contribute to seasonal profile of NRBI_{NIR} for soybean, whereas the nighttime cDN_{NIR} detected a seasonal change in the scattering property of soybean. This provides high sensitivity of NRBI_{NIR} in response to the SB+TLB. Sakamoto et al. (2011b) investigated the response of ISO sensitivity and nighttime cDN_{NIR} while varying the camera-to-object distances using a forklift. This study found that the night-time cDN_{NIR} also plays an important role to enhance

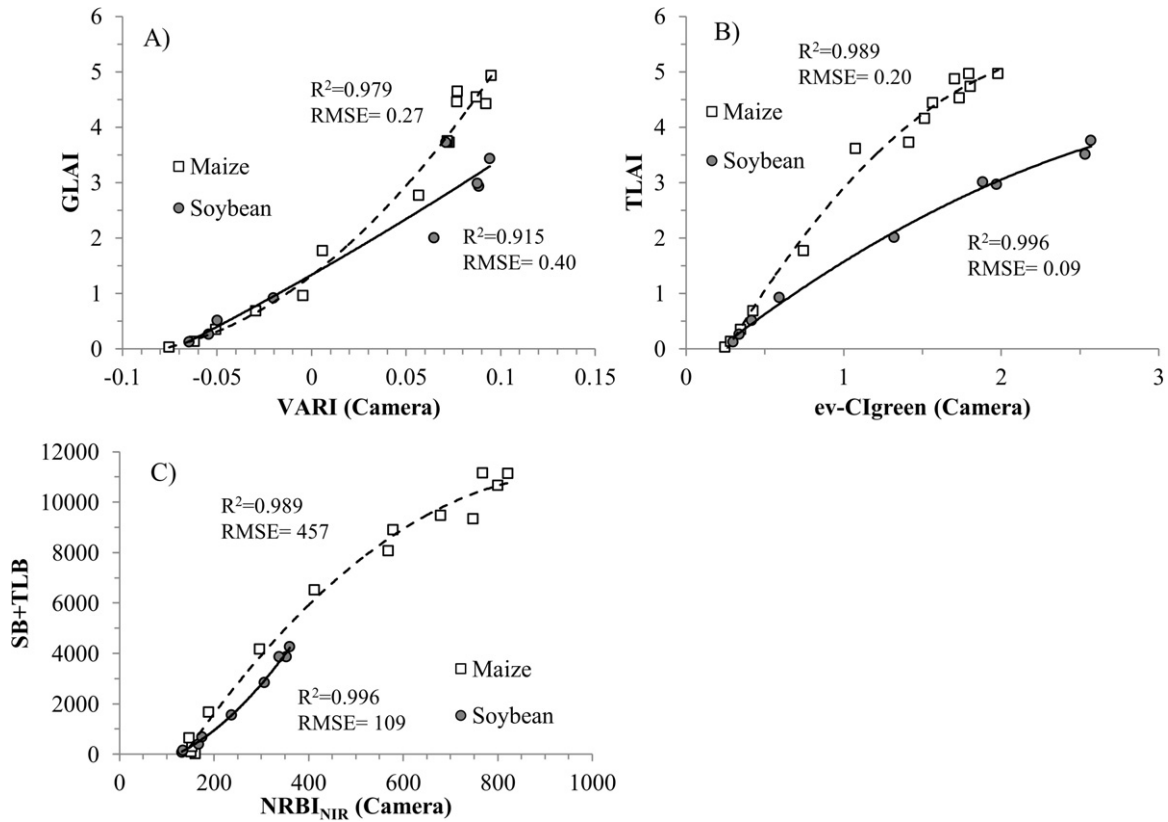


Fig. 9. Comparison between the ground-measured biophysical parameters (A: green LAI, B: total LAI, and C: above-ground dry biomass of stalks and leaves [i.e. excluding reproductive organs]) and the camera-derived indices (A: VARI, B: ev-CI_{green}, and C: NRBI_{NIR}).

Table 3

Summary of estimation accuracy of camera-derived VIs used to estimate *f*APAR of maize and soybean. The best estimation results are highlighted in bold style.

VI	Maize (DOY: 140–257, <i>n</i> = 118)			Soybean (DOY: 150–246, <i>n</i> = 97)			Maize + Soybean (<i>n</i> = 215)		
	R ²	CV (%)	RMSE	R ²	CV (%)	RMSE	R ²	CV (%)	RMSE
VARI	0.86	13.3	0.089	0.98	8.1	0.046	0.93	11.7	0.073
ev-NDVI	0.96	7.4	0.050	0.97	9.0	0.051	0.96	8.8	0.055
ev-SR	0.92	10.0	0.067	0.94	12.8	0.073	0.92	12.1	0.075
ev-CI _{green}	0.94	8.6	0.057	0.95	11.9	0.068	0.94	10.9	0.068
2g-r-b	0.95	8.3	0.055	0.98	7.6	0.043	0.96	8.4	0.052

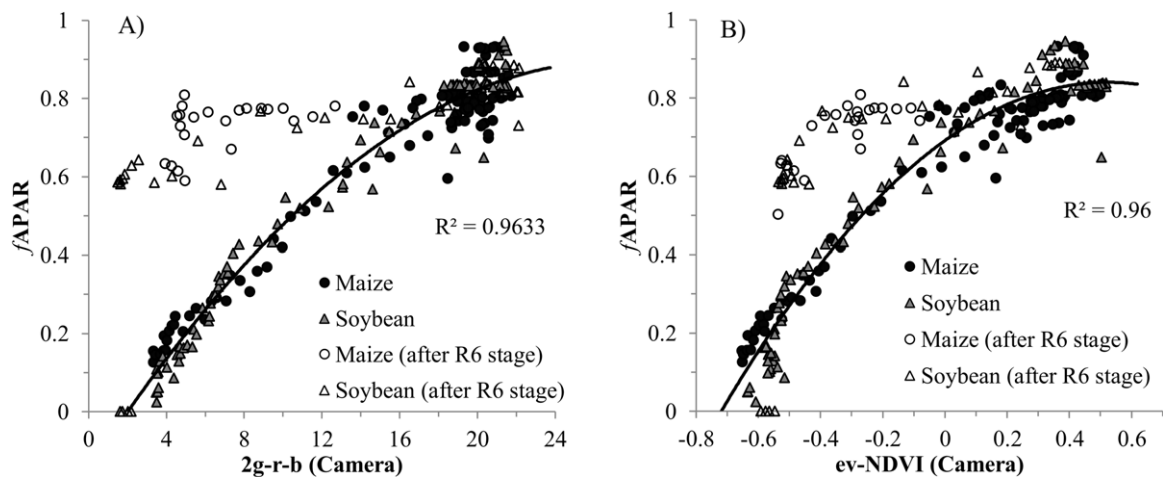


Fig. 10. Comparison between the ground-measured *f*APAR and the camera-derived indices (A: ev-NDVI and B: 2g-r-b).

the sensitivity of $NRBI_{NIR}$ in addition to ISO sensitivity. This study also revealed that the nighttime flash NIR images acquired by fixed point observation are effective for assessing the aboveground morphological parameter of soybean, which is difficult to estimate by remote sensing based on solar illumination. This is consistent with the cases of rice, barley (Sakamoto et al., 2010a), and maize (Sakamoto et al., 2011a).

4.5. Comparisons of the camera-derived VIs with *f*APAR

Crop *f*APAR shows a progressive increase during the vegetative stage until maximum canopy development, and then remains virtually invariant during the reproductive stage, with a decrease during the senescence stage. In the reproductive and senescence stages *f*APAR is insensitive to a decrease in crop chlorophyll content (Gitelson et al., 2005; Viña and Gitelson, 2005). Thus, vegetation indices, which are proxies of green LAI and chlorophyll content, relate closely to crop *f*APAR in vegetative stage. Camera-derived 2g-r-b showed the best estimation of daily *f*APAR in vegetative and early reproductive stages in maize (until DOY 257; R6 stage) and soybean (until DOY 246; R6 stage) (Table 3). It is marginally better than *ev*-NDVI when *f*APAR was estimated for both maize and soybean. As shown in Fig. 10, the quadratic approximations of the relationship *f*APAR vs. 2g-r-b are less subjected to being saturated than *ev*-NDVI. 2g-r-b and *ev*-NDVI are not species specific in estimating *f*APAR for morphologically different crops (maize and soybean) and their application does not require re-parameterization of the algorithms.

5. Conclusion

In this study, we ascertained if digital camera-derived vegetation indices have the potential to be alternative indicators of crop biophysical parameters to ground-based reflectance measurements. We explored the availability of day time exposure values recorded in the header region of EXIF-formatted JPEG files by RGB and NIR-cameras and proposed using vegetation indices, *ev*-NDVI, *ev*-SR, and *ev*- CI_{green} , which were calculated from the combination of daytime exposure values and *c*DN. The new findings are as follows:

1. The camera time series cDN_{green} and cDN_{NIR} were inconsistent with the spectral reflectance observations in terms of temporal behavior and seasonal dynamics. However, the new camera data, based on daytime exposure value in the green, red and NIR bands (*ev*-*c*DN), showed strong correlations with corresponding reflectance measured by two independent sensors: SKYE and MODIS.
2. Camera-derived *ev*- CI_{green} , *ev*-SR, and *ev*-NDVI showed strong linear correlations with corresponding vegetation indices derived from SKYE and MODIS. Camera-retrieved *ev*-NDVI was sensitive to wide range of green leaf area in both crops.
3. Performance of the digital camera-retrieved VIs in remote estimation of green LAI, green leaf biomass, total LAI and above-ground biomass excluding reproductive organs, was evaluated. This study found that *ev*-VARI worked the best for maize and *ev*- CI_{green} for soybeans when estimating green LAI. *ev*-VARI was also the best in estimating green leaf biomass in maize and $NRBI_{NIR}$ in soybean. Total LAI can be estimated accurately in both crops by *ev*-NDVI, *ev*-SR and *ev*- CI_{green} . Only $NRBI_{NIR}$ was able to accurately estimate the total biomass excluding reproductive organs in maize and soybean.
4. Camera-derived 2g-r-b showed the best accuracy in estimating daily *f*APAR in vegetative and early reproductive stages of both crops. The same quadratic approximate model may

have applicability to both maize and soybean not requiring re-parameterization.

Compact digital cameras are often remodeled in a short cycle (about six months to a year). Thus, it is difficult to use the same model for several years after a new camera product is released. Thus, when establishing the camera observation system with a new camera model, it is necessarily to conduct initial calibration of camera using spectral radiometers and verify the sensitivity of camera-retrieved vegetation indices to the biophysical parameters of interest. The photodiode-based optical methods (Gamon 2010; Garrity et al., 2010; Ryu et al., 2010) could provide a standard value of vegetation indices and reflectance to calibrate the camera system. Considering that camera-based vegetation indices have the possibility to estimate a wide variety of bio-physical parameters, we believe that fixed point camera observation would be an option for acquiring high-frequency observations of vegetation simultaneously in multiple locations.

Acknowledgements

The crop phenology recording system (CPRS) was manufactured by Kimura Oyo Kogei, Saitama, Japan. We gratefully acknowledge the facilities and equipment provided by the School of Natural Resources, University of Nebraska-Lincoln. We are grateful to Dr. Don Wilhite and Dr. Mike Hayes for supporting this research. We offer special thanks to Mr. Tom Lowman, Mr. Dave Soby, and Mr. Todd Schimelfenig for their technical support during field measurements. This work was partially supported by the Japanese Society for the Promotion of Science: JSPS Postdoctoral Fellowships for Research Abroad. We thank the anonymous reviewers for their valuable comments and suggestions.

References

- Adamsen, F.J., Pinter, P.J., Barnes, E.M., LaMorte, R.L., Wall, G.W., Leavitt, S.W., Kimball, B.A., 1999. Measuring wheat senescence with a digital camera. *Crop Science* 39 (3), 719–724.
- Ahrens, H.E., Etzold, S., Kutsch, W.L., Stoeckli, R., Bruegger, R., Jeanneret, F., Wanner, H., Buchmann, N., Eugster, W., 2009. Tree phenology and carbon dioxide fluxes: use of digital photography at for process-based interpretation the ecosystem scale. *Climate Research* 39 (3), 261–274.
- Betancourt, J., et al., 2005. Implementing a US national phenology network. *Eos Transactions on AGU* 86 (51), 539.
- Brown, M.E., de Beurs, K.M., 2008. Evaluation of multi-sensor semi-arid crop season parameters based on NDVI and rainfall. *Remote Sensing of Environment* 112 (5), 2261–2271.
- Delbart, N., Kergoat, L., Le Toan, T., Lhermitte, J., Picard, G., 2005. Determination of phenological dates in boreal regions using normalized difference water index. *Remote Sensing of Environment* 97 (1), 26–38.
- Demarez, V., Duthoit, S., Baret, F., Weiss, M., Deduc, G., 2008. Estimation of leaf area and clumping indexes of crops with hemispherical photographs. *Agricultural and Forest Meteorology* 148 (4), 644–655.
- Falkowski, M.J., Gessler, P.E., Morgan, P., Hudak, A.T., Smith, A., 2005. Characterizing and mapping forest fire fuels using ASTER imagery and gradient modeling. *Forest Ecology and Management* 217 (2–3), 129–146.
- Gamon, J.A., 2010. Integrating remote sensing and flux measurements. *Flux Letter* 3 (1), 7–10.
- Garrity, S.R., Vierling, L.A., Bickford, K., 2010. A simple filtered photodiode instrument for continuous measurement of narrowband NDVI and PRI over vegetated canopies. *Agricultural and Forest Meteorology* 150 (3), 489–496.
- Gitelson, A.A., 2004. Wide dynamic range vegetation index for remote quantification of biophysical characteristics of vegetation. *Journal of Plant Physiology* 161 (2), 165–173.
- Gitelson, A.A., Kaufman, Y.J., Stark, R., Rundquist, D., 2002. Novel algorithms for remote estimation of vegetation fraction. *Remote Sensing of Environment* 80 (1), 76–87.
- Gitelson, A.A., Vina, A., Ciganda, V., Rundquist, D.C., Arkebauer, T.J., 2005. Remote estimation of canopy chlorophyll content in crops. *Geophysical Research Letters* 32 (8).
- Hanan, N., Burba, G., Verma, S.B., Berry, J.A., Suyker, A.E., Walter-Shea, E.A., 2002. Inversion of net ecosystem CO₂ flux measurements for estimation of canopy PAR absorption. *Global Change Biology* (8), 563–574.

- Huete, A., Didan, K., Miura, T., Rodriguez, E.P., Gao, X., Ferreira, L.G., 2002. Overview of the radiometric and biophysical performance of the MODIS vegetation indices. *Remote Sensing of Environment* 83 (1–2), 195–213.
- Hunt, E.R., Hively, W.D., Fujikawa, S., Linden, D., Daughtry, C.S., McCarty, G., 2010. Acquisition of NIR-green-blue digital photographs from unmanned aircraft for crop monitoring. *Remote Sensing* 2 (1), 290–305.
- Islam, A.S., Bala, S.K., 2008. Assessment of potato phenological characteristics using MODIS-derived NDVI and LAI information. *Geoscience & Remote Sensing* 45 (4), 454–470.
- Jordan, C.F., 1969. Derivation of leaf-area index from quality of light on forest floor. *Ecology* 50 (4), 663–666.
- Lukina, E.V., Stone, M.L., Rann, W.R., 1999. Estimating vegetation coverage in wheat using digital images. *Journal of Plant Nutrition* 22 (2), 341–350.
- Matsuda, M., Ozawa, S., Hosaka, Y., Kaneda, K., Yamashita, H., 2003. Estimation of plant growth in paddy field based on proximal remote sensing—measurement of leaf nitrogen contents by using digital camera. *Journal of The Remote Sensing Society of Japan* 23 (5), 506–515.
- Meyer, G.E., Hindman, T.W., Laksmi, K., 1999. In: Meyer, G.E., DeShazer, J.A. (Eds.), *Machine Vision Detection Parameters for Plant Species Identification*. SPIE, Boston, MA, USA, pp. 327–335.
- Motohka, T., Nasahara, K.N., Oguma, H., Tsuchida, S., 2010. Applicability of green-red vegetation index for remote sensing of vegetation phenology. *Remote Sensing* 2 (10), 2369–2387.
- Nagai, S., Nasahara, K.N., Muraoka, H., Akiyama, T., Tsuchida, S., 2010. Field experiments to test the use of the normalized-difference vegetation index for phenology detection. *Agricultural and Forest Meteorology* 150 (2), 152–160.
- Nishida, K., 2007. Phenological eyes network (PEN)—a validation network for remote sensing of the terrestrial ecosystems. *Asia Flux Newsletter* (21), 9–13.
- Perez, A.J., Lopez, F., Benlloch, J.V., Christensen, S., 2000. Colour and shape analysis techniques for weed detection in cereal fields. *Computers and Electronics in Agriculture* 25 (3), 197–212.
- Reed, B.C., Brown, J.F., Vanderzee, D., Loveland, T.R., Merchant, J.W., Ohlen, D.O., 1994. Measuring phenological variability from satellite imagery. *Journal of Vegetation Science* 5 (5), 703–714.
- Richardson, A.D., et al., 2007. Use of digital webcam images to track spring green-up in a deciduous broadleaf forest. *Oecologia* 152 (2), 323–334.
- Rouse, J., 1974. Monitoring vegetation systems in the Great Plains with ERTS.
- Rundel, P.W., Graham, E.A., Hamilton, M.P., Mishler, B.D., Hansen, M.H., 2006. Use of a networked digital camera to estimate net CO₂ uptake of a desiccation-tolerant moss. *International Journal of Plant Sciences* 167 (4), 751–758.
- Ryu, Y., et al., 2010. Testing the performance of a novel spectral reflectance sensor, built with light emitting diodes (LEDs), to monitor ecosystem metabolism, structure and function. *Agricultural and Forest Meteorology* 150 (12), 1597–1606.
- Sakamoto, T., Gitelson, A.A., Wardlow, B.D., Arkebauer, T.J., Shashi, B.V., Suyker, A.E., Shibayama, M., 2011. Application of day and night digital photographs for estimating maize biophysical characteristics. *Precision Agriculture*, doi:10.1007/s11119-011-9246-1.
- Sakamoto, T., Shibayama, M., Kimura, A., Takada, E., 2011b. Assessment of digital camera-derived vegetation indices in quantitative monitoring of seasonal rice growth. *ISPRS Journal of Photogrammetry and Remote Sensing* 66 (6), 872–882.
- Sakamoto, T., Shibayama, M., Takada, E., Inoue, A., Morita, K., Takahashi, W., Miura, S., Kimura, A., 2010a. Detecting seasonal changes in crop community structure using day and night digital images. *Photogrammetric Engineering and Remote Sensing* 76 (6), 713–726.
- Sakamoto, T., Wardlow, B.D., Gitelson, A.A., 2011a. Detecting spatiotemporal changes of corn developmental stages in the US corn belt using MODIS WDRVI data. *IEEE Transactions on Geoscience and Remote Sensing* 49 (6), 1926–1936.
- Sakamoto, T., Wardlow, B.D., Gitelson, A.A., Verma, S.B., Suyker, A.E., Arkebauer, T.J., 2010b. A two-step filtering approach for detecting maize and soybean phenology with time-series MODIS data. *Remote Sensing of Environment* 114 (10), 2146–2159.
- Sakamoto, T., Yokozawa, M., Toritani, H., Shibayama, M., Ishitsuka, N., Ohno, H., 2005. A crop phenology detection method using time-series MODIS data. *Remote Sensing of Environment* 96 (3–4), 366–374.
- Schwartz, M.D., Reed, B.C., White, M.A., 2002. Assessing satellite-derived start-of-season measures in the conterminous USA. *International Journal of Climatology* 22 (14), 1793–1805.
- Shibayama, M., Sakamoto, T., Homma, K., Okadai, S., Yamamoto, H., 2009a. Daytime and nighttime field spectral imagery of ripening paddy rice for determining leaf greenness and 1000-grain weight. *Plant Production Science* 12 (3), 307–318.
- Shibayama, M., Sakamoto, T., Takada, E., Inoue, A., Morita, K., Takahashi, W., Kimura, A., 2009b. Continuous monitoring of visible and near-infrared band reflectance from a rice paddy for determining nitrogen uptake using digital cameras. *Plant Production Science* 12 (3), 293–306.
- Shibayama, M., Sakamoto, T., Takada, E., Inoue, A., Morita, K., Takahashi, W., Kimura, A., 2011. Estimating paddy rice leaf area index with fixed point continuous observation of near infrared reflectance using a calibrated digital camera. *Plant Production Science* 14 (1), 30–46.
- Tucker, C.J., 1979. Red and photographic infrared linear combinations for monitoring vegetation. *Remote Sensing of Environment* 8 (2), 127–150.
- Verma, S.B., Dobermann, A., Cassman, K.G., Walters, D.T., Knops, J.M., Arkebauer, T.J., Suyker, A.E., Burba, G.G., Amos, B., Yang, H.S., Ginting, D., Hubbard, K.G., Gitelson, A.A., Walter-Shea, E.A., 2005. Annual carbon dioxide exchange in irrigated and rainfed maize-based agroecosystems. *Agricultural and Forest Meteorology* 131 (1–2), 77–96.
- Viña, A., Gitelson, A.A., 2005. New developments in the remote estimation of the fraction of absorbed photosynthetically active radiation in crops. *Geophysical Research Letters* 32, L17403, doi:10.1029/2005GL023647.
- Vina, A., Gitelson, A.A., Rundquist, D.C., Keydan, G., Leavitt, B., Schepers, J., 2004. Remote sensing—monitoring maize (*Zea mays* L.) phenology with remote sensing. *Agronomy Journal* 96 (4), 1139–1147.
- Wardlow, B.D., Kastens, J.H., Egbert, S.L., 2006. Using USDA crop progress data for the evaluation of greenup onset date calculated from MODIS 250-m data. *Photogrammetric Engineering and Remote Sensing* 72 (11), 1225–1234.
- White, M.A., Thornton, P.E., Running, S.W., 1997. A continental phenology model for monitoring vegetation responses to interannual climatic variability. *Global Biogeochemical Cycles* 11 (2), 217–234.
- Woebbecke, D.M., Meyer, G.E., Vonbargen, K., Mortensen, D.A., 1995. Color indexes for weed identification under various soil, residue, and lighting conditions. *Transactions of the ASAE* 38 (1), 259–269.
- Xiao, X.M., Holinger, D., Aber, J., Goltz, M., Davidson, E.A., Zhang, Q.Y., Moore, B., 2004. Satellite-based modeling of gross primary production in an evergreen needle leaf forest. *Remote Sensing of Environment* 89 (4), 519–534.
- Zhang, X.Y., Friedl, M.A., Schaaf, C.B., Strahler, A.H., Hodges, J.C.F., Gao, F., Reed, B.C., Huete, A., 2003. Monitoring vegetation phenology using MODIS. *Remote Sensing of Environment* 84 (3), 471–475.